Impact of Metal Hybridization on Contact Resistance and Leakage Current of Carbon Nanotube Transistors

Sheng-Kai Su*, Alfonso Sanchez-Soares, Edward Chen, Thomas Kelly, Giorgos Fagas, James C. Greer, Gregory Pitner, Member, *IEEE*, H.-S. Philip Wong, *Fellow, IEEE*, and Iuliana P. Radu

***Abstract*—Carbon nanotube field effect transistors (CNFETs) have potential applications in future logic technology as they display good electrostatic control and excellent transport properties. However, contact resistance and leakage currents could limit scaling of CNFETs. Non-equilibrium Green's function (NEGF) simulation investigates that coupling between contact metal and CNT impacts both contact resistance and leakage current. The physical mechanisms underlying the effects are analyzed. A model with calibrated metal coupling strength from experimental data projects I_{ON}-I_{OFF} design space to understand the trade-off between shrinking contact and extension lengths. For CNT with diameter of 1 nm, both contact and extension lengths greater than 8 nm are a good compromise between I_{ON} and I_{OFF} for digital logic in advanced technology nodes.**

***Index Terms*—Carbon nanotube (CNT), CMOS scaling, contact resistance, leakage current, metal hybridization.**

I. Introduction

CONTINUOUS transistor scaling in lateral dimensions faces challenges for silicon technology [1]. High mobility carbon nanotube (CNT) carrying large on-state currents in a small area is promising for next generation transistors [2]. However, the large on-state currents are associated with small effective mass and bandgap which results in undesirable leakage in the off-state. Previous studies have shown that Schottky barrier CNT field effect transistors (SB-CNFETs) at high drain bias have strong ambipolar conduction by Schottky tunneling that sets the floor for minimum off-state leakage [3-5]. This tunneling is expected to be suppressed in CNT transistor with a MOSFET structure that has doped extensions spatially isolating channel from Schottky contacts. For this structure, band-to-band tunneling (BTBT) becomes the main mechanism setting the floor of the off-state current [5, 6]. To our knowledge, the impact of and interplay between contact design and leakage mechanisms have not been understood yet. In this work, we discuss the effect of metal-CNT hybridization on contact resistance and Schottky tunneling leakage. We find that Schottky tunneling cannot be ignored even in a CNT MOSFET and must be considered along with contact resistance for CNT digital logic transistors in advanced technology nodes.

"This work was supported by Taiwan Semiconductor Manufacturing Company." *(Corresponding author: Sheng-Kai Su.)*

S.K. Su, E. Chen, and I. P. Radu are with the Corporate Research, Taiwan Semiconductor Manufacturing Company (TSMC), Hsinchu 30075, Taiwan (e-mail: sksua@tsmc.com).

A. Sanchez-Soares, and T. Kelly are with EOLAS Designs Ltd, Grenagh, Co. Cork T23 AK70, Ireland.

G. Fagas is with the Tyndall National Institute, University College Cork, Cork T12 R5CP, Ireland.

J.C. Greer is with the Electrical and Electronic Engineering Department, University of Nottingham Ningbo China, Ningbo 315100, China.

G. Pitner, and H.-S. P. Wong are with Corporate Research, Taiwan Semiconductor Manufacturing Company, San Jose CA 95134, USA.

H.-S. P. Wong is with the Department of Electrical Engineering, Stanford University, Stanford CA 94305, USA.

II. Simulation Approach

A coupled mode-space non-equilibrium Green's function (NEGF) solver with a k.p electronic Hamiltonian [7] is employed to simulate the electrical properties of CNFETs arranged in arbitrary 3D geometries [8]. Periodic boundary conditions are applied along the width dimension to simulate nanotube arrays. Physical quantities are explicitly computed throughout the device channel and extension leads by a self-consistent loop solving Poisson's and Schrödinger's equations, and computing the retarded Green's function given by

$$G(E) = [(E + i\eta)I - H - \Sigma]^{-1},$$

where E is the energy, η is an infinitesimal positive value, I the identity matrix, H the CNT Hamiltonian, and $\Sigma = \Sigma_{PH} + \Sigma_{S/D}$ a self-energy term describing both phonon scattering and coupling to the source/drain (S/D) contacts. Elastic and inelastic scattering mediated by acoustic and optical phonon modes are included using the formalism and parameters described in [9]. Carrier flow between the extension leads and S/D electrodes is described by Schottky contacts at metal-CNT interfaces with input metal Fermi energy. Models for both end- and side-bonded contacts are evaluated. End contacts are modeled by coupling extension leads to self-energies computed using metallic CNT Hamiltonians [4]. Coupling to side contacts is described through self-energy terms computed using a CNT Hamiltonian with the same chirality as the channel's and with finite contact length L_C, wherein metal hybridization is modeled by inclusion of an energy-independent diagonal term $-i\Delta$ describing coupling to a wideband metal with strength Δ [10, 11]. In this description, carrier injection process between contact and CNT is treated in the ballistic limit, which has been reported to be a good approximation for CNTs with long mean free path [12]. Tunning of both chemical and geometrical parameters allows exploration of the impact of contacts on

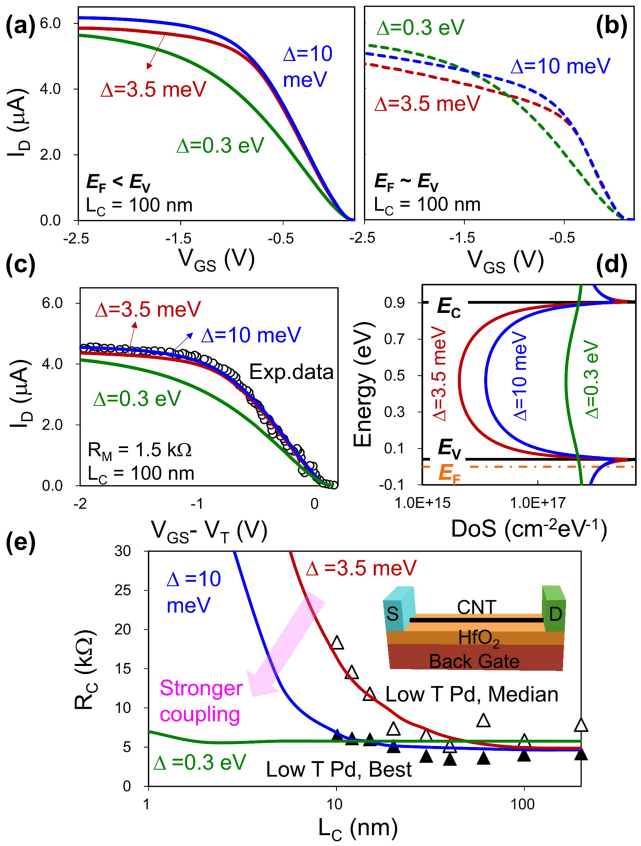

Fig. 1. (a),(b) I_D-V_{GS} for strong (Δ=0.3 eV, green), medium (Δ=10 meV, blue), and weak (Δ=3.5 meV, red) metal coupling strength with (a) metal Fermi energy E_F ~40 meV lower than valence band edge E_V of CNT and (b) $E_F \sim E_V$. (c) Same condition as (a) except for metal-wire resistance R_M=1.5 kΩ included for data (symbol) comparison [14]. The drain bias applied is -50 mV and contact length L_C is 100 nm. (d) Energy-dependent density of states (DOS) of CNT in the contact portion for different metal coupling strengths. (e) Contact resistance R_C per CNT per contact as a function of L_C. Lines: simulation results for different metal coupling strengths; symbols: best (filled) and median (open) experimental R_C from [14]. Inset: The simulated SB-CNFET structure, which is the same as experimental device structure of [14], with back gate length 50 nm and 5 nm HfO_2 gate dielectric.

device performance. In this work, a representative wrap-around contact (WAC) geometry in which the CNT is completely covered by the contact metal was used.

Devices studied in this work are based on (13,0) zigzag CNTs with ~1 nm diameter and a ~0.86 eV band gap which is shown to be a good compromise between I_{ON} and I_{OFF} [6, 13]. To facilitate connection to experimental results, we report here on p-type transistors with a metal Fermi level aligned near the valence band edge of CNT. Given the electron-hole symmetry present in the employed CNT Hamiltonian, all results reported in this work are also applicable to n-type transistors.

III. Results and Discussions

The degree of hybridization between metal and CNT impacts contact resistance significantly. Figure 1a and 1b compares I_D-V_{GS} of a SB-CNFET (inset of fig.1e) for contacts with different metal-CNT hybridization and different S/D metal Fermi energy. For small coupling strength Δ, the current and its slope to V_{GS} (i.e., transconductance G_m) is larger at low gate bias; at high (more negative) gate bias, the current started to

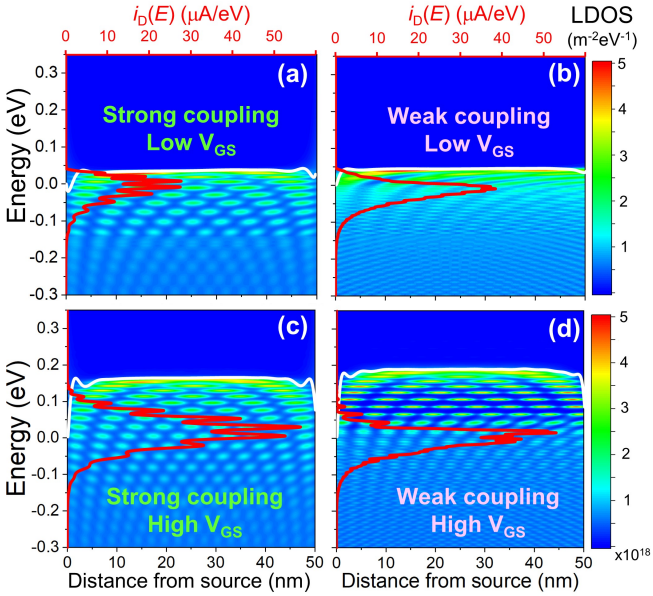

Fig. 2. Local density of states (LDOS, color), valence band edge (white line) and energy resolved current $i_D(E)$ (red line, top *x*-axis) for strong Δ=0.3 eV (a, c) and weak Δ=3.5 meV (b, d) coupling strength at low (a, b) and high (c, d) back gate bias corresponding to V_{GS}= -0.5 V and -2.0 V in fig. 1b. The metal Fermi energy aligns with the CNT valence band edge and is set to 0 eV at the source side.

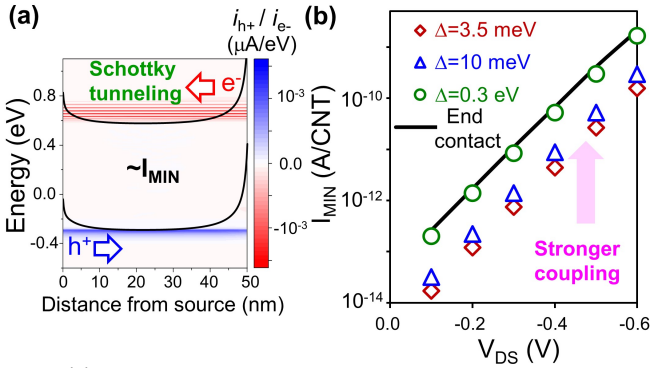

Fig. 3. (a) The band diagram and energy-position resolved electron and hole current at V_{GS} around minimum current I_{MIN}, which is the lowest off-state current limited by ambipolar conduction due to Schottky tunneling. (b) I_{MIN} versus V_{DS} for wrap-around (side-bonded) contact with different metal coupling strengths (symbol) and end-bonded contact (line). The same device structure is used as in fig. 1.

saturate with G_m becomes lower and more sensitive to the S/D metal Fermi energy compared to the case of strong coupling. To compare with experimental data, contact resistance R_C is extracted following the same method as from the experiment [14]. $2R_C$ is assumed equal to total resistance at high overdrive -2 V due to small contribution of channel resistance of short channel CNFET [14]. The dependence of R_C to contact length L_C for different metal hybridization is shown in fig. 1e. The simulated R_C becomes more immune to L_C scaling for stronger metal-CNT coupling.

To understand the results, analyses of the local density of states (LDOS) and energy resolved current spectrum for different coupling strength and V_{GS} are shown in fig. 2. The metal Fermi energy near valence band edge of CNT in the contact portion is set to zero at source (fig. 1d). For low gate bias, carriers injected at the source traverse the channel at energies near the valence band edge in the channel (fig. 2a, b).

For strong coupling (fig. 2a), because of the DOS mismatch between the channel and the "metalized" CNT in the contact (fig. 1d), the channel LDOS exhibits strong state quantization, and corresponding oscillations in the energy-resolved current spectrum are shown. Thus, weak coupling results in better contact transparency than strong coupling at low gate bias. Once the gate bias becomes larger (more negative for pFET) and the valence band edge of the CNT in the channel moves away from the metal Fermi level towards higher energies (fig. 2c, d), carriers can transport at energies deep inside the band gap of the CNT in the contact portion. This relies on the induced states inside the bandgap. For weak hybridization, the availability of metal induced gap states (MIGS) at energies far away from the valence band edge is limited leading to "source starvation" with small injection current at high energies shown in fig. 2d. In contrast, abundant MIGS in the case of strong hybridization supports carrier injection resulting in the current spectrum across an extensive energy range (fig. 2c). This reduces R_C at high channel carrier density and lowers sensitivity of R_C to the metal Fermi energy for strong compared to weak hybridization contacts.

Metal hybridization also impacts R_C to L_C dependence. As the coupling strength increases, a side-bonded contact behaves more like an end-bonded contact with shorter transfer length. This is because the larger amount of MIGS induced by stronger interacting metals makes the portion of the CNT in the contact more "metallic-like" (fig. 1d). The simulated I_D-V_{GS} (fig. 1c) and R_C-L_C (fig. 1e) reproduce experimental data [14] using appropriate empirical coupling strength Δ and contact metal Fermi energy. The obtained parameters of the best Pd-CNT contact data are used to carry out performance projections discussed later.

In addition to contact resistance, metal-CNT hybridization affects Schottky tunneling leakage current. Unlike S/D reservoirs assumed in earlier studies [3-5], the DOS of the side-contacted CNT depends on contact geometry and metal hybridization. For WAC, the Fermi level of the CNT within the metal contact is fixed near the valence band edge and difficult to modulate by a back gate bias. Thus, the Schottky tunneling of ambipolar carriers (electrons for pFETs as shown in fig. 3a) relies on the MIGS in the contact portion of the CNT. Figure 3b shows the minimum current I_{MIN} of SB-CNFETs as a function of V_{DS} with different metal-CNT coupling strengths. The I_{MIN} for WAC increases for stronger metal-CNT hybridization and approaches that of devices with end-bonded contacts. This is consistent with the R_C to L_C dependence discussed above.

We finally address the effect of metal-CNT hybridization on CNT MOSFETs (fig. 4a). The use of doped extensions in MOSFETs, is expected to suppress ambipolar leakage [3-5]. However, for scaled MOSFETs with extension length shorter than Schottky tunneling distance, ambipolar leakage can be large, making it essential to carefully design the device dimensions. For a constant contacted gate pitch (CGP) of 45 nm (fig. 4a) and to avoid serious direct source-to-drain tunneling leakage (fig. 4b) [15, 16], 12 nm gate length with a doping density ~0.4 nm^{-1} induced by dopants in the bottom dielectric is assumed. A power supply voltage of 0.5 V is used to mitigate BTBT (fig. 4b) for ~1 nm diameter CNTs [6]. A metal-CNT coupling strength Δ=10 meV is used based on the calibration of

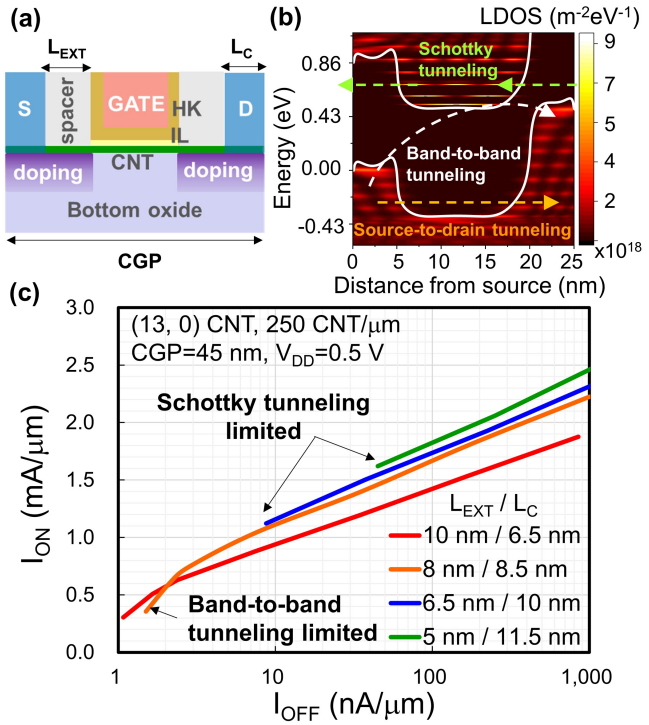

Fig. 4. (a) Cross-section of the simulated CNT MOSFET with defined contacted gate pitch (CGP), contact length L_C and extension length L_{EXT}. (b) LDOS and band diagram with schematic leakage mechanisms of a CNT MOSFET. (c) I_{ON} versus I_{OFF} for different L_{EXT}/L_C at constant CGP of 45 nm. Simulation parameters: 0.5 nm/1.5 nm Al_2O_3/HfO_2 gate stack, 4 nm CNT pitch, coupling strength Δ=10 meV, and 0.5 V power supply voltage V_{DD}.

the data of low-temperature fabricated Pd-CNT contacts [14]. Because metal hybridization affects both contact resistance and Schottky tunneling leakage, the trade-off between contact length L_C and extension length L_{EXT} on I_{ON} and I_{OFF} is shown in fig. 4c. The decrease in contact resistance resulting from increasing L_C (fig. 1c) increases I_{ON}, but the associated reduction of L_{EXT} increases I_{OFF} because of strong Schottky tunneling leakage that can even dominate over BTBT for L_{EXT} < 8 nm. Increasing L_{EXT} suppresses Schottky tunneling leakage, but the accompanying L_C reduction degrades I_{ON} due to rapidly increasing R_C.

IV. Conclusions

The DOS of the CNT in the contact depends on contact geometry and metal-CNT hybridization. Strong hybridization degrades contact transparency, but the resulting abundant MIGS supports carrier injection across an extensive energy range. This reduces contact resistance at high doping density but results in strong ambipolar leakage, which cannot be ignored for scaled MOSFETs. Based on the metal coupling strength extracted from the comparison to experimental data, we propose both extension and contact lengths longer than 8 nm to compromise between standby power tuning range and performance for different applications of CNT MOSFETs with CNT diameter ~1 nm. The results could be significant for scaling potential assessment of CNFET for digital logic in advanced technology nodes.

REFERENCES

[1] S. K. Su, C. P Chuu, M. Y Li, C. C. Cheng, H.-S. P. Wong, and L. J. Li, "Layered semiconducting 2D materials for future transistor applications," *Small Struct.*, vol. 2, no. 5, p. 2000103, Jan. 2021, doi: 10.1002/sstr.202000103.

[2] A. Javey, J. Guo, Q. Wang, M. Lundstrom, and H. Dai, "Ballistic carbon nanotube field-effect transistors," *Nature*, vol. 424, no.6949, pp. 654-657, Aug. 2003, doi: 10.1038/nature01797.

[3] A. Javey, J. Guo, D. B. Farmer, Q. Wang, D. Wang, R. G. Gordon, M. Lundstrom, and H. Dai, "Carbon nanotube field-effect transistors with integrated ohmic contacts and high-κ gate dielectrics," *Nano Letters*, vol. 4, no. 3, pp. 447-450, Feb. 2004, doi: 10.1021/nl035185x.

[4] J. Guo, S. Datta, and M. Lundstrom, "A numerical study of scaling issues for Schottky-barrier carbon nanotube transistors," *IEEE Trans. Electron Dev.*, vol. 51, no. 2, pp. 172-177, Jan, 2004, doi: 10.1109/TED.2003.821883.

[5] J. Guo, A. Javey, H. Dai, S. Datta, and M. Lundstrom, "Predicted performance advantages of carbon nanotube transistors with doped nanotubes as source/drain," arXiv preprint cond-mat/0309039, 2003.

[6] Q. Lin, G. Pitner, C. Gilardi, S. K. Su, Z. Zhang, E. Chen, P. Bandaru, A. Kummel, H. Wang, M. Passlack, S. Mitra, and H.-S. Philip Wong, "Bandgap extraction at 10 K to enable leakage control in carbon nanotube MOSFETs," *IEEE Electron Device Lett.*, Vol. 43, no. 3, pp. 490-493, Mar. 2022, doi: 10.1109/LED.2022.3141692.

[7] H. Ajiki, and T. Ando, "Electronic states of carbon nanotubes," *J. Phys. Soc. Japan*, vol. 62, no. 4, pp. 1255-1266, Apr. 1993, doi: 10.1143/JPSJ.62.1255.

[8] EOLAS proprietary TCAD tool Q*, https://eolasdesigns.com, Nov. 2021.

[9] S. O. Koswatta, S. Hasan, M. Lundstrom, M. P. Anantram, and D. E. Nikonov, "Nonequilibrium green's function treatment of phonon scattering in carbon-nanotube transistors," *IEEE Trans. Electron Dev.*, vol. 54, no. 9, pp. 2339-2351, Oct. 2007, doi: 10.1109/TED.2007.902900.

[10] N. Nemec, D. Tománek, and G. Cuniberti, "Contact dependence of carrier injection in carbon nanotubes: an ab initio study," *Phys. Rev. Lett.*, vol. 96, no. 7, p. 076802, Feb. 2006, doi: 10.1103/PhysRevLett.96.076802.

[11] N. Nemec, D. Tománek, and G. Cuniberti, "Modeling extended contacts for nanotube and graphene devices," *Phys. Rev. B, Condens. Matter*, vol. 77, no. 12, p. 125420, Mar. 2008, doi: 10.1103/PhysRevB.77.125420.

[12] F. Xia, V. Perebeinos, Y. Lin, Y. Wu and P. Avouris, "The origins and limits of metal–graphene junction resistance," *Nat. Nanotechnol.*, vol. 6, pp. 179-184, Mar. 2011, doi: 10.1038/nnano.2011.6.

[13] Z. Chen, J. Appenzeller, J. Knoch, Y. M. Lin, and P. Avouris, "The role of metal-nanotube contact in the performance of carbon nanotube field-effect transistors," *Nano Letters*, vol. 5, no. 7, pp. 1497-1502, Jun. 2005, doi: 10.1021/nl0508624.

[14] G. Pitner, G. Hills, J. P. Llinas, K.-M. Persson, R. Park, J. Bokor, S. Mitra, and H.-S. P. Wong, "Low-Temperature side contact to carbon Nanotube Transistors: Resistance Distributions down to 10 nm Contact Length," *Nano Letters*, vol. 19, no. 2, pp. 1083–1089, Jan. 2019, doi: 10.1021/acs.nanolett.8b04370.

[15] S. K. Su, E. Chen, T. Y. T. Hung, M. Z. Li, G. Pitner, C. C. Cheng, H. Wang, J. Cai, H.-S. P. Wong, and I. P. Radu, "Perspective on Low-dimensional Channel Materials for Extremely Scaled CMOS," *2022 IEEE VLSI Symposium on Technology and Circuits*, T14-4, Jun. 2022.

[16] C. S. Lee, E. Pop, A. D. Franklin, W. Haensch, and H.-S. P. Wong, "A compact virtual-source model for carbon nanotube FETs in the sub-10-nm regime—Part II: Extrinsic elements, performance assessment, and design optimization," *IEEE Trans. Electron Dev.*, vol. 62, no. 9, pp. 3070-3078, Aug. 2015, doi: 10.1109/TED.2015.2457424.